diagnostics

MDPI

Article

PET and Magnetization Transfer MRI for Early Prediction of Neoadjuvant Chemotherapy Response in Breast Cancer

Lo-Yi Lin [1,2], Yu Kuo [3], Yi-Fang Tsai [2,4], Ling-Ming Tseng [2,4], Ko-Han Lin [5,6], Tiffany Ting-Fang Shih [7] and Jane Wang [1,7,8,*]

1 Department of Radiology, Taipei Veterans General Hospital, No. 201, Sec. 2, Shipai Rd., Beitou Dist., Taipei 112201, Taiwan; zoelin061@gmail.com
2 School of Medicine, College of Medicine, National Yang Ming Chiao Tung University, No. 155, Sec. 2, Linong St. Beitou Dist., Taipei 112304, Taiwan; yftsai@vghtpe.gov.tw (Y.-F.T.); lmtseng@vghtpe.gov.tw (L.-M.T.)
3 Division of Radiology, Taipei Municipal Gan-Dau Hospital, No. 12, Ln. 225, Zhixing Rd., Beitou Dist., Taipei 112020, Taiwan; ucs198604@gmail.com
4 Department of Surgery and Comprehensive Breast Health Center, Taipei Veterans General Hospital, No. 201, Sec. 2, Shipai Rd., Beitou Dist., Taipei 112201, Taiwan
5 Department of Nuclear Medicine, Taipei Veterans General Hospital, No. 201, Sec. 2, Shipai Rd., Beitou Dist., Taipei 112201, Taiwan; khlin1979@gmail.com
6 Department of Medical Imaging and Radiological Sciences, Chung Shan Medical University, No. 110, Sec. 1, Jianguo North Road, Taichung 40201, Taiwan
7 Department of Radiology, National Taiwan University College of Medicine, No. 1, Jen Ai Rd., Sec. 1, Taipei 100233, Taiwan; ttfshih@ntu.edu.tw
8 Department of Nurse-Midwifery and Women Health, School of Nursing, College of Nursing, National Taipei University of Nursing and Health Sciences, No. 365, Ming-Te Rd., Beitou Dist., Taipei 112303, Taiwan
* Correspondence: jwwangjen@gmail.com or jwang2@vghtpe.gov.tw; Tel.: +886-2-2871-2121 (ext. 21181)

Abstract

Background/Objectives: Early assessment of response to neoadjuvant chemotherapy (NAC) may facilitate treatment evaluation in breast cancer. We evaluated the performance of PET SUV-based and MRI-derived magnetization transfer ratio (MTR) metrics for early prediction of NAC response. **Methods:** From January 2019 to December 2021, 30 women with newly diagnosed breast cancer (mean age, 46.6 ± 11.2 years) scheduled for NAC underwent hybrid FDG PET/MR. Participants received two examinations: study 1 before NAC, and study 2 during early NAC (mean, 18.2 ± 4.6 days after NAC initiation). PET metrics included SUVmax of the index tumor (SUVlesion) and SUVs measured in ipsilateral and contralateral normal breast parenchyma (SUVipsi, SUVcontra). MTR metrics included MTRlesion encompassing the SUVmax site, with MTRipsi and MTRcontra in normal breast parenchyma. Ratios (SUVlesion/ipsi, SUVlesion/contra, MTRlesion/ipsi, MTRlesion/contra) were also calculated. Treatment response was categorized as residual cancer burden (RCB) 0–I (group 1) or II–III (group 2). ROC analysis with leave-one-out cross-validation was performed. **Results:** Group 1 showed greater reductions in imaging metrics, whereas group 2 showed smaller reductions or increases (percent changes: all Δ%SUV metrics, $p \leq 0.001$; Δ%MTRlesion and Δ%MTRlesion/ipsi, $p \leq 0.013$). SUV-based metrics generally demonstrated higher diagnostic performance than MTR metrics (AUC, 0.652–0.864 vs. 0.656–0.756), with the highest AUC among individual metrics observed for Δ%SUVlesion/ipsi. Selected hybrid SUV-MTR metrics showed numerically higher AUCs than the corresponding individual metrics, with the highest AUC (0.919) achieved by Δ%MTRlesion/ipsi combined with SUVlesion at study 2. **Conclusions:** In this exploratory pilot study, SUV-based metrics showed higher overall diagnostic performance than MTR-based metrics for early prediction of NAC response. Selected hybrid metrics yielded numerically higher AUCs than individual metrics; these preliminary findings require validation in larger cohorts.

Check for updates

Academic Editor: Takouhie Catherine Maldjian

Received: 26 October 2026
Revised: 18 November 2026
Accepted: 20 November 2026
Published: 23 November 2026

Copyright: © 2026 by the authors. Licensee MDPI, Basel, Switzerland. This article is an open access article distributed under the terms and conditions of the Creative Commons Attribution (CC BY) license.

Keywords: breast cancer; PET; magnetization transfer imaging; neoadjuvant chemotherapy

1. Introduction

Neoadjuvant chemotherapy (NAC) is widely used in patients with breast cancer to reduce tumor burden and increase the probability of breast-conserving surgery [1–9]. Early prediction of treatment response to NAC is clinically imperative because it may allow timely modification of therapeutic strategies and potentially improve clinical outcomes [1–10]. Both F-18 fluorodeoxyglucose (FDG) positron emission tomography (PET) and magnetic resonance imaging (MRI) have demonstrated value for early assessment of NAC response in breast cancer [1–9,11–15]. Previous studies have evaluated semiquantitative PET parameters including standardized uptake value (SUV), metabolic tumor volume (MTV), and total lesion glycolysis (TLG), as well as MRI-derived metrics from dynamic contrast-enhanced (DCE) MRI, diffusion-weighted imaging (DWI) with apparent diffusion coefficient (ADC) maps, and magnetic resonance spectroscopy (MRS) [1–9,11–15]. These imaging biomarkers have demonstrated predictive value for NAC response, with reported areas under the receiver operating characteristic curve (AUCs) of 0.68–0.93 for FDG PET and 0.79–0.90 for MRI-based approaches [1–7,9,11–14]. Combined PET and MRI assessments have also been investigated for NAC response prediction, with reported AUCs ranging from 0.78 to 0.98 [1–7,9–11,13,14].

Magnetization transfer imaging (MTI), quantified by the magnetization transfer ratio (MTR), reflects interactions between free water protons and protons associated with macromolecular pools, and may provide insight into tissue microstructure [16–21]. While widely studied in neurologic disorders [19–21], MTI has been explored only to a limited extent in breast imaging, including applications in lesion characterization and studies in healthy volunteers [16–18]. A prior study of breast cancer patients undergoing NAC reported no significant change in mean tumoral MTR during treatment. Histogram-based analysis, however, revealed significantly increased dispersion of MTR values during treatment, suggesting greater intratumoral heterogeneity, particularly in patients achieving pathologic complete response (pCR) [22]. FDG PET-derived parameters and MTR-derived metrics reflect different aspects of tumor biology; however, their relative performance for early prediction of NAC response remains unclear.

The purpose of this exploratory study was to investigate the performance of PET- and MTR-derived parameters, as well as their combination, for early prediction of NAC response using hybrid PET/MR imaging in patients with breast cancer.

2. Materials and Methods

2.1. Patients

This prospective study was approved by the institutional review board of the hospital's Research Ethics Committee, and written informed consent was obtained from all participants.

From January 2019 to December 2021, 36 women with newly diagnosed breast cancer who were scheduled to receive NAC underwent PET/MR examinations. Two patients were excluded because pretreatment MTI was unavailable. Four additional patients were excluded because of incomplete serial PET/MR examinations ($n = 2$), absence of surgery ($n = 1$), or severe motion artifacts ($n = 1$). Thus, 30 women (age range, 30–74 years; mean age, 46.6 ± 11.2 years) were included in the final analysis (Figure 1). All 30 patients had invasive ductal carcinoma and clinical stage IIA disease or higher according to the American Joint Committee on Cancer staging system (8th edition) before NAC. During patient screen-

ing, women with an estimated glomerular filtration rate (eGFR) <60 mL/min/1.73 m^2 or fasting blood glucose levels >135 mg/dL were excluded.

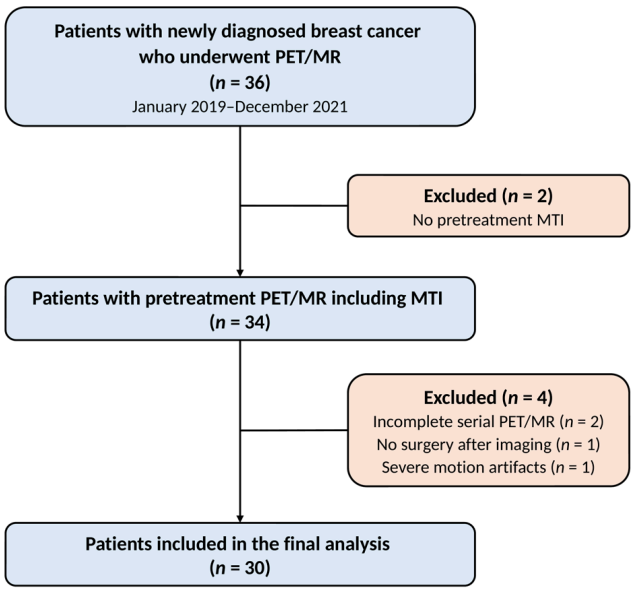

Figure 1. Flowchart of patient selection. MTI, magnetization transfer imaging; PET/MR, positron emission tomography/magnetic resonance imaging.

NAC regimens included taxane-based chemotherapy (docetaxel, paclitaxel, or nab-paclitaxel) combined with carboplatin (or cisplatin) followed by an anthracycline-based regimen (epirubicin or adriamycin) with cyclophosphamide, or the reverse sequence. For patients with triple-negative breast cancer (TNBC) expressing programmed cell death-1 (PD-1) or programmed cell death-ligand 1 (PD-L1), immune checkpoint inhibitors (pembrolizumab or atezolizumab) were administered concurrently with chemotherapy. For human epidermal growth factor receptor 2 (HER2)-positive tumors, either a taxane-based regimen with carboplatin and dual-targeted therapy (trastuzumab and pertuzumab) or a taxane-based regimen with trastuzumab followed by an anthracycline-based regimen with cyclophosphamide were given.

2.2. Imaging Protocol

All patients underwent hybrid PET/MR examinations on a PET/MR scanner (Signa PET/MR, GE HealthCare, Waukesha, WI, USA) with patients in the prone position using a dedicated 8-channel breast coil. Participants fasted for at least 6 h before the PET/MR examination. After intravenous administration of 3–4 MBq/kg of FDG, patients rested for approximately 60 min before each PET/MR study. A 10 min breast PET acquisition was performed in a single-bed position together with precontrast breast MRI. PET images were reconstructed using a 3D time-of-flight ordered-subset expectation maximization algorithm (2 iterations, 28 subsets). Attenuation correction of PET data was obtained from a 4-tissue-class segmented attenuation map (air, lung, fat, and soft tissue) generated by a liver acceleration volume acquisition (LAVA, Dixon-based) MRI.

The MRI protocol included precontrast axial non-fat-suppressed T1-weighted imaging, T2-weighted short-tau inversion recovery (STIR) imaging, and magnetization transfer imaging (MTI). DCE MRI consisted of one precontrast and six postcontrast acquisitions using a 3D fat-suppressed sequence (volume imaging for breast assessment [VIBRANT]; TR/TE 7.9/4.3 ms; flip angle 10°; slice thickness/gap 1/0 mm; field of view 320 × 320 mm; matrix: 320 × 224). A gadolinium-based contrast agent (gadoteric acid, Dotarem; Guerbet,

Cedex, France) was administered intravenously at 0.1 mmol/kg at a rate of 2.5 mL/s. In this study, we focused quantitative MRI analysis on MTI, whereas DCE MRI and other sequences were used for routine clinical interpretation and to assist in identifying the index tumors and confirming normal breast tissue regions for ROI placement.

For MTI, MTR measurements were derived from a chemical exchange saturation transfer (CEST) acquisition performed using a two-dimensional single-shot fast spin-echo sequence with a 1.5 s continuous Gaussian-shaped pulse (root-mean-square B1, 1.6 μT). Imaging parameters were as follows: repetition time, 6.8 s; effective echo time, 32 ms; bandwidth, ±62.5 kHz; matrix, 160 × 160; field of view, 24 × 24 cm^2; and slice thickness, 6 mm. Images were acquired at 29 frequency offsets ranging from −7 to +7 ppm, with an additional reference acquisition performed without a saturation pulse. For MTR calculation, the signal acquired with saturation at +7 ppm was used as the saturated signal (Ssat), and the signal acquired without saturation was used as the reference signal (S0). Three axial slices were obtained, with the center slice corresponding to the level of the lesion SUVmax and a 10 mm interslice gap.

The magnetization transfer ratio (MTR) was calculated as follows:

$$\mathrm{MTR} = 1 - (\mathrm{Ssat}/\mathrm{S0}) \quad (1)$$

Two PET/MR examinations were performed for each participant: study 1 was performed before NAC and study 2 during the early phase of NAC, at a mean of 18.2 days (SD 4.6 days) after the first chemotherapy dose.

2.3. Imaging Analysis

On PET, SUV-based metrics included SUVlesion, SUVipsi, and SUVcontra. SUVlesion represented the SUVmax of the index tumor. SUVipsi and SUVcontra were measured from circular ROIs (diameter, 4 mm) placed in relatively compact fibroglandular areas of ipsilateral and contralateral normal breast parenchyma. The ratios of SUVlesion/ipsi and SUVlesion/contra were calculated as lesion-to-ipsilateral and lesion-to-contralateral SUV ratios, respectively.

MTR-based metrics included MTRlesion, MTRipsi, and MTRcontra. MTRlesion was measured from a circular ROI (diameter, 4 mm) placed within the index tumor with reference to the SUVmax location. MTRipsi and MTRcontra were obtained from ROIs placed in corresponding fibroglandular areas of ipsilateral and contralateral normal breast parenchyma, aiming for close anatomical correspondence with PET-derived ROIs. The ratios of MTRlesion/ipsi and MTRlesion/contra were calculated as lesion-to-ipsilateral and lesion-to-contralateral MTR ratios, respectively.

In our study, a fixed ROI diameter of 4 mm was used for all ROI-based measurements to standardize sampling across patients and between tumor and normal breast tissues. This size was selected as a practical compromise between obtaining localized measurements and avoiding the inclusion of adjacent fat, particularly in elongated tumors or areas with limited fibroglandular tissue. Normal tissue ROIs used for PET and MTR measurements were verified to show no abnormal enhancement on DCE MRI.

Percent changes (Δ%) of SUV- and MTR-based metrics were calculated as follows:

$$[(\text{metric in study 1} - \text{metric in study 2})/\text{metric in study 1}] \times 100\%$$

ROIs were defined by a dual board-certified radiologist (diagnostic radiology and nuclear medicine) with 5 years of experience in PET/MR interpretation, under the supervision of a breast radiologist with 15 years of experience in breast MRI and 9 years in breast PET/MR. Dedicated analysis software (MANGO version 4.1; Research Imaging Institute, University of Texas Health Science Center, San Antonio, TX, USA) was used with technical

assistance from two imaging scientists (GE HealthCare) for quantitative data extraction and organization. An illustration of ROI placement is shown in Figure 2.

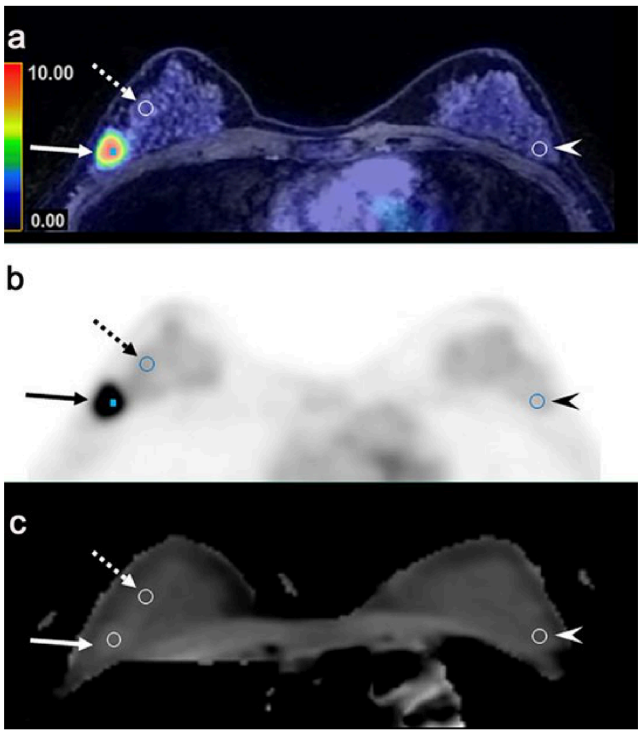

Figure 2. A patient with right breast cancer before neoadjuvant chemotherapy. Illustration of PET and MTR ROI placement. (**a**) Fused axial PET/MR image and (**b**) axial PET image demonstrate the index tumor (solid arrow), with SUVmax indicated by a blue square; ROIs (white circles in (**a**) and blue circles in (**b**)) are placed in the ipsilateral (dashed arrow) and contralateral (arrowhead) normal breast parenchyma. (**c**) MTR measurements show corresponding ROIs (white circles) in the index tumor (solid arrow), as well as in ipsilateral (dashed arrow) and contralateral (arrowhead) normal breast parenchyma. MTR, magnetization transfer ratio.

2.4. Pre-NAC Clinicopathological Characteristics

Pre-NAC clinicopathological variables included patient age, clinical T and N stage, MRI tumor size of the index cancer (largest diameter), and core biopsy findings (Ki-67, estrogen receptor [ER], progesterone receptor [PR], HER2 status, and histologic grade). Ki-67 ≥ 20% was considered high-risk [23]. HER2 status was assessed by immunohistochemistry (IHC) (3+ positive, 0/1+ negative); equivocal 2+ cases underwent fluorescence in situ hybridization (FISH), with amplification confirming positivity. Tumors were classified as TNBC-like if ER and PR were both <10% and HER2-negative, given their clinical similarity to TNBC (ER < 1%, PR < 1%, HER2-negative) [24]. Accordingly, ER and PR were categorized as ≥10% or <10%; tumors with both <10% were hormone receptor (HR)-negative, and all others HR-positive. Composite subtypes included HR(+)/HER2(−), HR(+)/HER2(+), HR(−)/HER2(+), and TNBC-like.

2.5. Assessment of NAC Response

Treatment response to NAC was determined according to surgical pathology after completion of NAC. Patients were classified according to residual cancer burden (RCB). Group 1 represented better response (RCB class 0 or I), whereas group 2 represented poorer response (RCB class II or III). RCB class was calculated using the MD Anderson Cancer Center online calculator (https://www3.mdanderson.org/app/medcalc/index.cfm?pagename=jsconvert3) (accessed on 25 October 2026).

2.6. Statistical Analysis

For the overall cohort, age and the interval between the two examinations are presented as mean ± standard deviation. Given the small sample size, nonparametric tests were used for group comparisons. Continuous variables, including patient age, tumor size, SUV- and MTR-based metrics at studies 1 and 2, and their percent changes, were summarized as medians with ranges and compared between groups 1 and 2 using the Mann–Whitney *U* test. Categorical variables, including T and N stage, histologic grade, ER/PR/HER2 status, Ki-67 status, and tumor subtypes, were compared using Fisher's exact test. Imaging metrics were compared according to receptor status and TNBC-like subtype using the Mann–Whitney *U* test, and across the four subtypes using the Kruskal–Wallis test. Receiver operating characteristic (ROC) analysis was performed for SUV- and MTR-based metrics showing significant differences between the two response groups, with RCB II–III defined as the positive outcome. Logistic regression models were constructed using individual imaging metrics or hybrid combinations of SUV- and MTR-based metrics. Given the limited sample size, predictive performance was evaluated using leave-one-out cross-validation (LOOCV), in which each patient was held out once for prediction, and ROC curves were generated from the cross-validated predicted probabilities. The area under the ROC curve (AUC) and its 95% confidence interval were estimated using the DeLong method. To prioritize sensitivity, the cutoff yielding the highest accuracy among those achieving sensitivity >80% was selected. Sensitivity, specificity, positive predictive value (PPV), negative predictive value (NPV), and accuracy were then calculated using this cutoff. A p value < 0.05 was considered statistically significant. All statistical analyses were performed using SPSS Statistics (version 25; IBM Corp., Armonk, NY, USA) and Stata/SE 19 (StataCorp LLC, College Station, TX, USA).

3. Results

3.1. Patient Characteristics and NAC Response

Among the 30 patients included in the study, 13 were classified into group 1 (RCB 0–I), including 10 patients with pCR (RCB class 0), and 17 into group 2 (RCB II–III). Pre-NAC clinicopathologic characteristics of the two groups are summarized in Table 1. Breast cancers in group 1 were more frequently associated with low ER and PR expression (ER < 10% and PR < 10%) compared with those in group 2 ($p = 0.017$ and $p = 0.010$, respectively). In addition, subtype distribution differed significantly between the two groups ($p = 0.003$), with all HR(−)/HER2(+) tumors observed in group 1, whereas HR(+) cancers were more frequently categorized into group 2. Patient age, index tumor size measured by MRI, clinical T and N stage, histologic grade, HER2 status, and Ki-67 index did not differ significantly between the two groups.

Table 1. Pre-NAC basic characteristics of the study participants.

	Group 1 ($n = 13$)	**Group 2 ($n = 17$)**	***p***
Age, years	42 (30–74)	49 (30–62)	0.50
MRI tumor size (cm)	3.6 (1.8–7.9)	5.1 (1.6–11.6)	0.13
	n (%)	*n* (%)	
Clinical T staging			0.25
1	0 (0)	1 (5.9)	
2	10 (76.9)	8 (47.1)	
3	3 (23.1)	5 (29.4)	
4	0 (0)	3 (17.6)	

Table 1. *Cont.*

	Group 1 (n = 13)	Group 2 (n = 17)	p
Clinical N staging			0.19
0	2 (15.4)	2 (11.8)	
1	9 (69.2)	6 (35.3)	
2	1 (7.7)	2 (11.8)	
3	1 (7.7)	7 (41.1)	
Histologic grade			0.26
I/II (non-high)	6 (46.2)	12 (70.6)	
III (high)	7 (53.8)	5 (29.4)	
ER expression			0.017
ER < 10%	12 (92.3)	8 (47.1)	
ER ≥ 10%	1 (7.7)	9 (52.9)	
PR expression			0.010
PR < 10%	13 (100)	10 (58.8)	
PR ≥ 10%	0 (0)	7 (41.2)	
HER2 status			0.13
HER2(−)	6 (46.2)	13 (76.5)	
HER2(+)	7 (53.8)	4 (23.5)	
Ki67			0.49
Ki67 < 20%	0 (0)	2 (11.8)	
Ki67 ≥ 20%	13 (100)	15 (88.2)	
Composite subtype			0.003
HR(+)/HER2(−)	0 (0)	5 (29.4)	
HR(+)/HER2(+)	1 (7.7)	4 (23.5)	
HR(−)/HER2(+)	6 (46.2)	0 (0)	
TNBC-like	6 (46.2)	8 (47.1)	

The age and MRI tumor size are shown as median (range) and compared using the Mann–Whitney *U* test. Group 1: Residual cancer burden (RCB) class 0 or I; group 2: RCB class II or III. ER, estrogen receptor; PR, progesterone receptor; HER2, human epidermal growth factor receptor-2. HR, hormone receptor. HR(−) indicates both ER and PR < 10%, otherwise HR(+). TNBC-like: triple-negative breast cancer-like. The clinical staging, histologic grade, ER, PR expression, HER2 status, Ki67, and composite subtype are shown as number (n) and percent (%) and compared using Fisher's exact test.

3.2. SUV- and MTR-Based Metrics According to NAC Response

The SUV-based parameters between groups 1 and 2 are summarized in Table 2 and Figure 3. Group 1 patients demonstrated significantly larger reductions in lesion SUVmax (Δ%SUVlesion, $p < 0.001$), SUVlesion/ipsi (Δ%SUVlesion/ipsi, $p < 0.001$), and SUVlesion/contra (Δ%SUVlesion/contra, $p = 0.001$) compared with group 2. In addition, selected PET-SUV parameters at study 2 were also significantly lower in group 1, including SUVlesion ($p = 0.003$) and SUVlesion/ipsi ($p = 0.025$), suggesting a more pronounced early metabolic response among patients with better NAC outcomes.

Table 2. SUV- and MTR-based metrics between group 1 and 2 patients.

	Group 1 (n = 13)	Group 2 (n = 17)	p
SUV-based metrics †			
Lesion			
1st	12.8 (4.2–15.6)	10.6 (2.9–27.4)	0.98
2nd	3.3 (2.0–7.5)	6.6 (2.2–27.9)	0.003
Δ%SUVlesion	69.6 (37.2–85.5)	36.6 (−30.2–74.0)	<0.001
Lesion/Ipsi			
1st	7.9 (2.8–34.7)	7.0 (1.7–23.8)	0.57
2nd	2.8 (1.5–9.6)	5.1 (1.2–28.9)	0.025
Δ%SUVlesion/ipsi	68.2 (24.1–80.6)	27.2 (−21.7–52.6)	<0.001

Table 2. *Cont.*

	Group 1 (n = 13)	Group 2 (n = 17)	p
Lesion/Contra			
1st	8.9 (2.8–39.0)	7.7 (2.5–41.8)	0.82
2nd	2.6 (1.3–16.0)	4.8 (1.7–38.1)	0.05
Δ%SUVlesion/contra	61.9 (23.6–80.9)	38.6 (−49.5–69.1)	0.001
MTR-based metrics			
Lesion			
1st	1.2 (0.2–2.1)	0.3 (0.2–2.0)	0.41
2nd	0.3 (0.1–1.7)	0.3 (0.2–2.3)	0.63
Δ%MTRlesion	8.2 (−3.6–93.3)	−8.0 (−1228.7–92.8)	0.013
Lesion/Ipsi			
1st	1.2 (0.9–2.4)	1.2 (0.6–2.3)	0.33
2nd	1.0 (0.8–2.4)	1.3 (0.8–2.3)	0.11
Δ%MTRlesion/ipsi	11.7 (−3.7–55.6)	−7.1 (−88.5–25.2)	0.004
Lesion/Contra			
1st	1.2 (1.0–2.3)	1.2 (0.7–7.3)	0.44
2nd	1.1 (0.7–1.5)	1.2 (0.7–2.5)	0.27
Δ%MTRlesion/contra	8.5 (−16.4–70.2)	3.5 (−72.4–66.2)	0.49

All values are presented as median (range). All p values were calculated using the Mann–Whitney U test. † Lesion SUV (SUVlesion) was defined as the SUVmax of the index tumor. SUV of ipsilateral and contralateral normal breast tissues and all MTR metrics were derived from ROIs. The 1st study indicates the pre-NAC PET/MR examination. The 2nd study indicates the PET/MR examination performed during the early cycle of NAC. Δ% indicates the percent change of the corresponding parameter from the 1st to the 2nd study. SUVlesion/ipsi and SUVlesion/contra represent lesion-to-ipsilateral and lesion-to-contralateral SUV ratios, respectively. MTRlesion/ipsi and MTRlesion/contra represent lesion-to-ipsilateral and lesion-to-contralateral MTR ratios, respectively.

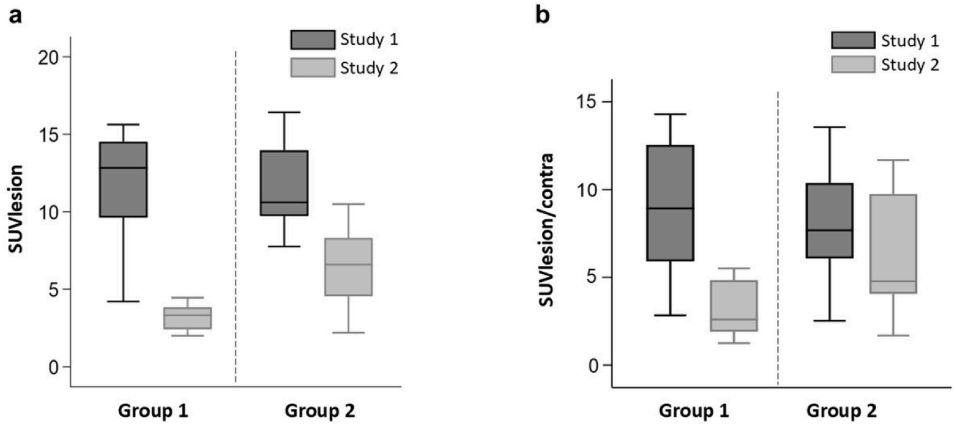

Figure 3. Box plots of selected PET-SUV parameters in groups 1 and 2. Patients in group 1 showed greater reductions in (**a**) SUVlesion and (**b**) SUVlesion/contra than those in group 2 ($p < 0.001$ and $p = 0.001$ for percent changes, respectively). SUVlesion, SUVmax of the index tumor; SUVlesion/contra, ratio of lesion SUVmax to SUV of contralateral normal breast tissue. Group 1, RCB class 0–I; group 2, RCB class II–III.

Regarding MTR-derived metrics between the two groups (Table 2), group 1 tended to show reductions in MTR-based parameters, whereas group 2 showed increasing trends in selected MTR metrics from study 1 to study 2. This pattern was observed for both Δ%MTRlesion (median = 8.2% vs. −8.0% for groups 1 and 2, respectively, $p = 0.013$) and Δ%MTRlesion/ipsi (median = 11.7% vs. −7.1% for groups 1 and 2, respectively, $p = 0.004$). Other imaging parameters did not differ significantly between the two groups of patients.

3.3. Predictive Performance of Individual and Hybrid Imaging Metrics

We further evaluated the diagnostic performance of imaging metrics that showed significant group differences (Table 2) for predicting NAC response. The ROC analysis results are presented in Tables 3 and 4 and Figure 4. Among the individual metrics, SUV-based parameters showed AUCs ranging from 0.652 to 0.864, with the highest observed for Δ%SUVlesion/ipsi. Sensitivity ranged from 82.4 to 100%, with NPVs of 66.7–100%, and accuracies of 66.7–86.7% based on the optimal cutoff points. In comparison, AUCs for MTR-based metrics ranged from 0.656 to 0.756, with sensitivities of 82.4–94.1%, NPVs of 50.0–66.7%, and accuracies of 56.7–66.7% based on the optimal cutoff values. Hybrid markers integrating both SUV- and MTR-based metrics demonstrated AUCs ranging from 0.783 to 0.919 (Table 4), with sensitivities of 82.4% to 94.1%, NPVs of 72.7% to 90.9%, and accuracies of 70.0% to 86.7% using the optimal cutoff values. The highest observed AUC was 0.919 for the model combining Δ%MTRlesion/ipsi and SUVlesion at study 2. Hybrid models incorporating Δ%MTRlesion/ipsi consistently showed numerically higher AUCs than the corresponding individual markers, whereas those incorporating Δ%MTRlesion showed more variable performance relative to individual SUV-based metrics. Notably, combining Δ%MTRlesion/ipsi with single time-point SUV-based metrics (SUVlesion or SUVlesion/ipsi at study 2) yielded AUCs of ≥0.891, despite the relatively lower individual AUCs of these SUV-based metrics.

Table 3. ROC analysis of individual SUV- and MTR-based metrics for predicting NAC response.

	AUC (95% CI)	Sen%	Spe%	PPV%	NPV%	Acc%
SUV-based metrics						
Δ%SUVlesion	0.828 (0.670–0.986)	82.4	76.9	82.3	77.0	80.0
Δ%SUVlesion/ipsi	0.864 (0.720–1.000)	100.0	69.2	80.9	100.0	86.7
Δ%SUVlesion/contra	0.805 (0.632–0.979)	88.2	69.2	78.9	81.8	80.0
SUVlesion 2nd	0.765 (0.577–0.953)	88.2	46.2	68.2	75.0	70.0
SUVlesion/ipsi 2nd	0.652 (0.445–0.858)	82.4	46.2	66.7	66.7	66.7
MTR-based metrics						
Δ%MTRlesion	0.656 (0.453–0.860)	94.1	7.7	57.1	50.0	56.7
Δ%MTRlesion/ipsi	0.756 (0.580–0.931)	82.4	46.2	66.7	66.7	66.7

The ROC analysis was performed using leave-one-out cross-validation. The optimal cutoff was defined as the threshold with the highest accuracy among those achieving sensitivity >80%. Sen: sensitivity; Spe: specificity; PPV: positive predictive value; NPV: negative predictive value; Acc: accuracy. The abbreviations and definitions for SUV- and MTR-based metrics are the same as those in Table 2.

Table 4. ROC analysis of hybrid SUV-MTR models for predicting NAC response.

	AUC (95% CI)	Sen%	Spe%	PPV%	NPV%	Acc%
Δ%MTRlesion + Δ%SUVlesion	0.783 (0.609–0.957)	82.4	61.5	73.7	72.7	73.3
Δ%MTRlesion + Δ%SUVlesion/ipsi	0.842 (0.684–1.000)	94.1	76.9	84.2	90.9	86.7
Δ%MTRlesion + Δ%SUVlesion/contra	0.805 (0.636–0.975)	82.4	76.9	82.3	77.0	80.0
Δ%MTRlesion + SUVlesion 2nd	0.801 (0.631–0.970)	88.2	61.5	75.0	80.0	76.7
Δ%MTRlesion + SUVlesion/ipsi 2nd	0.796 (0.630–0.963)	88.2	46.2	68.2	75.0	70.0
Δ%MTRlesion/ipsi + Δ%SUVlesion	0.842 (0.681–1.000)	88.2	76.9	83.3	83.3	83.3
Δ%MTRlesion/ipsi + Δ%SUVlesion/ipsi	0.878 (0.745–1.000)	88.2	84.6	88.2	84.6	86.7
Δ%MTRlesion/ipsi + Δ%SUVlesion/contra	0.860 (0.723–0.997)	94.1	69.2	80.0	90.0	83.3
Δ%MTRlesion/ipsi + SUVlesion 2nd	0.919 (0.816–1.000)	94.1	76.9	84.2	90.9	86.7
Δ%MTRlesion/ipsi + SUVlesion/ipsi 2nd	0.891 (0.764–1.000)	88.2	84.6	88.2	84.6	86.7

The ROC analysis and cutoff definition were identical to those described in Table 3. Abbreviations are the same as those in Tables 2 and 3.

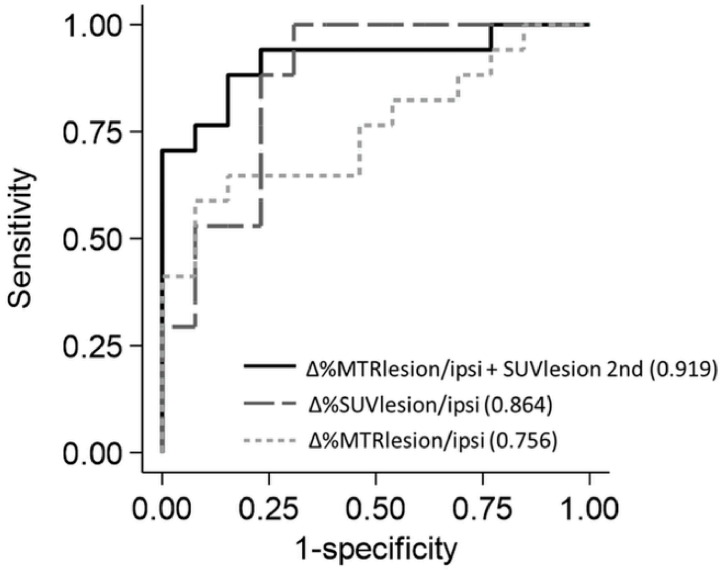

Figure 4. Receiver operating characteristic (ROC) curves for predicting response to neoadjuvant chemotherapy. The hybrid PET/MR metric (Δ%MTRlesion/ipsi + SUVlesion at study 2) showed the highest diagnostic performance among the metrics presented, followed by the best SUV-based metric (Δ%SUVlesion/ipsi) and MTR-based metric (Δ%MTRlesion/ipsi). AUC values are shown in parentheses. SUVlesion/ipsi, ratio of lesion SUVmax to SUV of ipsilateral normal breast tissue; MTRlesion/ipsi, ratio of lesion MTR to MTR of ipsilateral normal breast tissue. Δ% indicates the percent change of the corresponding parameter from the 1st to the 2nd study.

3.4. Imaging Metrics Stratified by Receptor Status and Tumor Subtype

SUV- and MTR-based metrics stratified by receptor status and TNBC-like subtype are summarized in Table 5. HER2-positive cancers demonstrated significantly lower SUV-based metrics at study 2 than HER2-negative counterparts ($p = 0.023$–0.045), along with significantly greater reductions in these parameters ($p = 0.009$–0.017). HER2-positive tumors showed lower MTRlesion/ipsi at study 2 ($p = 0.045$), without a significant difference in percent change. Breast cancers with ER < 10% showed significantly higher SUVlesion/ipsi, MTRlesion, and MTRlesion/ipsi at study 1 ($p = 0.048$, 0.031, and 0.039, respectively). MTRlesion/ipsi tended to decrease in ER < 10% tumors but increase in ER ≥ 10% tumors ($p = 0.006$ for Δ%MTRlesion/ipsi). Cancers with PR < 10% also showed higher MTRlesion ($p = 0.006$) and MTRlesion/ipsi ($p = 0.020$) at study 1. TNBC-like cancers showed higher MTRlesion/ipsi and MTRlesion/contra at study 1 ($p = 0.046$ and $p = 0.031$, respectively). Comparisons across composite subtypes are summarized in Table S1. HR(−)/HER2(+) cancers showed the greatest percent changes in the three SUV-based metrics ($p = 0.007$–0.010). Similar findings were observed for Δ%MTRlesion/ipsi ($p = 0.027$).

Table 5. SUV- and MTR-based metrics stratified by receptor status and TNBC-like subtype.

	ER			**PR**			**HER2**			**TNBC-like**		
	ER < 10% (*n* = 20)	**ER ≥ 10% (*n* = 10)**	***p***	**PR < 10% (*n* = 23)**	**PR ≥ 10% (*n* = 7)**	***p***	**HER2(−) (*n* = 19)**	**HER2(+) (*n* = 11)**	***p***	**TNBC-like (*n* = 14)**	**Non-TNBC-like (*n* = 16)**	***p***
SUV-based metrics												
Lesion												
1st	12.88	9.42	0.08	12.83	9.80	0.45	12.83	10.71	0.65	12.88	10.26	0.11
2nd	4.06	5.30	0.79	3.84	6.03	0.34	6.17	3.09	0.023	6.29	3.73	0.09
Δ%SUVlesion	66.50	43.60	0.09	62.20	58.20	0.36	40.40	67.90	0.009	55.80	64.60	0.43

Table 5. *Cont.*

	ER			PR			HER2			TNBC-like		
	ER < 10% (*n* = 20)	**ER ≥ 10% (*n* = 10)**	***p***	**PR < 10% (*n* = 23)**	**PR ≥ 10% (*n* = 7)**	***p***	**HER2(−) (*n* = 19)**	**HER2(+) (*n* = 11)**	***p***	**TNBC-like (*n* = 14)**	**Non-TNBC-like (*n* = 16)**	***p***
Lesion/Ipsi												
1st	8.07	5.51	0.048	7.90	5.53	0.27	7.39	7.48	0.88	8.07	6.14	0.17
2nd	4.12	3.92	0.79	3.92	4.02	0.51	4.85	2.76	0.045	5.06	3.37	0.07
Δ%SUVlesion/ipsi	53.80	33.00	0.05	52.40	38.90	0.12	34.40	58.90	0.017	38.30	49.60	0.48
Lesion/Contra												
1st	9.34	5.95	0.12	8.93	6.08	0.54	9.04	6.48	0.40	9.79	6.47	0.15
2nd	4.33	4.43	0.66	4.06	4.77	0.45	4.83	2.52	0.037	5.13	2.67	0.06
Δ%SUVlesion/contra	57.70	44.70	0.19	55.50	44.80	0.34	38.60	61.50	0.011	43.10	54.40	0.17
MTR-based metrics												
Lesion												
1st	0.76	0.23	0.031	0.60	0.18	0.006	0.29	0.28	0.64	0.29	0.27	0.14
2nd	0.30	0.30	0.76	0.31	0.25	0.39	0.29	0.31	0.53	0.28	0.68	0.80
Δ%MTRlesion	4.60	−16.50	0.08	4.50	−22.90	0.12	−0.90	8.00	0.40	0.70	0.60	0.41
Lesion/Ipsi												
1st	1.27	0.98	0.039	1.25	0.97	0.020	1.25	1.09	0.36	1.29	1.05	0.046
2nd	1.13	1.16	1.00	1.14	1.13	0.54	1.25	0.98	0.045	1.27	1.03	0.18
Δ%MTRlesion/ipsi	5.30	−18.4	0.006	4.10	−20.7	0.06	1.20	4.90	0.62	3.60	0.01	0.36
Lesion/Contra												
1st	1.20	1.12	0.31	1.21	1.07	0.34	1.21	1.19	0.27	1.30	1.13	0.031
2nd	1.14	1.05	0.63	1.19	1.00	0.48	1.24	1.00	0.10	1.27	1.03	0.17
Δ%MTRlesion/contra	7.10	7.50	0.86	6.50	9.00	0.71	3.50	8.50	0.68	3.20	8.80	0.80

All the imaging metrics are shown as median values. All the *p* values were evaluated by the Mann–Whitney *U* test. The definitions of SUV- and MTR-based metrics are the same as those in Table 2. All the abbreviations are the same as those in Tables 1 and 2.

4. Discussion

In this exploratory pilot study, we evaluated the diagnostic performance of PET-derived SUV metrics and MRI-derived MTR metrics for early prediction of treatment response to NAC. Most SUV-based metrics demonstrated higher diagnostic performance than MTR-based metrics in this context. Hybrid markers combining SUV- and MTR-based metrics, particularly those incorporating Δ%MTRlesion/ipsi, showed numerically higher AUCs (up to 0.919), suggesting that metabolic and macromolecular imaging biomarkers may provide complementary information for predicting treatment response.

Among the individual SUV-derived metrics reflecting tumor metabolic activity, several percent-change parameters showed moderate to good predictive performance (AUCs 0.805–0.864). Previous studies reported AUCs ranging from approximately 0.78 to 0.898 for Δ%SUVmax and from 0.789 to 0.878 for Δ%TLG when comparing baseline PET with early or mid-cycle imaging [2,5,9,12]. In contrast, SUV-based metrics measured at study 2 showed relatively limited performance (AUC 0.652–0.765). These findings suggest that dynamic changes in semiquantitative PET parameters may provide greater predictive value than measurements obtained at a single time point.

Although MTR has been shown to differ between malignant and benign breast lesions, its role in predicting response to NAC remains unclear [17,18,22]. A prior study reported no significant changes in tumoral MTR across serial time points, including pre-NAC and early-to-mid treatment cycles, with treatment effects instead reflected by increased MTR heterogeneity on histogram analysis [22]. In contrast, our ROI-based approach showed that percent changes in MTR-based metrics differed between the two response groups as early as the first NAC cycle. Group 1 (good responders, RCB 0–I) showed greater reductions in MTR metrics, whereas group 2 (RCB II–III) showed smaller reductions or even increases. These findings may reflect more prominent early remodeling of tumor macromolecular content in good responders. These preliminary results suggest that longitudinal changes in simplified MTR metrics may provide useful information for early prediction of treatment response.

Regarding hybrid PET/MR markers, previous studies have mainly combined PET parameters with MRI metrics derived from DCE MRI, DWI with ADC maps, and MRS, which reflect tumor perfusion, angiogenesis, water diffusivity, and choline composition [1–5,7,9,10,12,14]. In the present study, we incorporated MRI-derived MTR metrics, which provide information about macromolecular content and tissue integrity [17–22]. When combined with SUV-based metrics, selected MTR-related metrics were associated with numerically higher AUCs for predicting NAC response. In particular, the greater improvement observed with Δ%MTRlesion/ipsi than with Δ%MTRlesion is consistent with its better individual predictive performance. Interestingly, although single time-point SUV-based metrics (SUVlesion and SUVlesion/ipsi at study 2) showed limited individual performance, their combination with Δ%MTRlesion/ipsi yielded the two highest AUCs in this study. This finding suggests that these single time-point SUV metrics may provide complementary information when combined with MTR-based parameters, potentially capturing aspects of tumor response not fully reflected by percent-change SUV metrics within hybrid models.

Associations between imaging metrics and receptor status or tumor subtype were evaluated separately for SUV- and MTR-based metrics. For SUV-based metrics, HER2-positive tumors showed greater reductions than HER2-negative tumors, consistent with their higher response rates to NAC, particularly in HR(−)/HER2(+) tumors. Tumors with ER or PR < 10% tended to show higher SUVlesion at study 1, consistent with prior reports [25], whereas SUVlesion/ipsi at study 1 was significantly higher in tumors with ER <10%, suggesting greater sensitivity of this ratio-based metric. TNBC-like tumors also tended to show higher baseline SUVlesion, supporting the predictive value of PET-based metabolic metrics reported in the literature [25–27].

For MTR-based metrics, HER2-positive tumors showed lower MTRlesion/ipsi values at study 2, suggesting treatment-related changes. Baseline MTRlesion and MTRlesion/ipsi were higher in tumors with ER or PR < 10% than in those with ER or PR ≥ 10%. During treatment, however, both metrics decreased in ER/PR < 10% tumors but increased in ER/PR ≥ 10% tumors. TNBC-like tumors also tended to show higher baseline MTR-based metrics. These findings suggest that tumors with ER/PR < 10%, often associated with more aggressive subtypes such as HR(−)/HER2(+) or TNBC-like cancers, may exhibit differences in tumor microenvironment and higher NAC response rates. Additionally, subtype distribution differed significantly between the response groups, and treatment regimens varied according to subtype. These factors may have confounded the observed associations between imaging metrics and treatment response. Consequently, the independent predictive value of the imaging metrics remains uncertain.

Differences in imaging protocols and measurement techniques may affect the comparability of quantitative imaging metrics across studies. SUV measurements may vary with uptake time, reconstruction methods, and attenuation correction [28,29]. In addition, MTR values depend on saturation parameters and acquisition techniques, including differences between CEST-based and conventional MT imaging [22]. Although all examinations in our study were performed using the same scanner and acquisition protocol, the quantitative values and cutoff points derived from our findings may not be directly applicable to other scanners or protocols.

Several limitations should be acknowledged. First, the relatively small sample size reduced statistical power. To address this limitation, we used leave-one-out cross-validation to assess predictive performance while maximizing the data available for model training. However, the small sample size also limited our ability to assess potential confounding by receptor status, tumor subtype, and NAC regimens. Second, selection of ROIs in ipsilateral and contralateral normal breast tissue may introduce some subjectivity, and interobserver

reproducibility was not assessed. Identifying suitable fibroglandular tissue for ROI placement may be particularly challenging in patients with predominantly fatty breasts or large or multicentric tumors. In addition, the small fixed ROI (4 mm in diameter) may not fully capture whole-tumor heterogeneity. Future studies using whole-tumor segmentation and histogram analysis may provide a more comprehensive assessment. Third, although efforts were made to align the MTR ROI in the tumor with the lesion SUVmax location on PET, SUVmax represents a point estimate whereas MTR analysis is ROI-based. Therefore, the two measurements may reflect different spatial extents of the lesion. Finally, MTR was not compared with established quantitative MRI biomarkers, such as DCE-derived parameters or ADC. Future studies comparing these imaging biomarkers may help clarify the additional predictive value of MTR.

5. Conclusions

In this exploratory pilot study, PET-SUV metrics generally showed higher predictive performance than MTR metrics for early prediction of NAC response in breast cancer. Selected hybrid SUV- and MTR-based metrics showed numerically higher predictive performance than individual metrics. Given the small sample size, these findings should be considered preliminary and require validation in larger, independent cohorts.

Supplementary Materials: The following supporting information can be downloaded at: https://www.mdpi.com/article/10.3390/diagnostics16233933/s1, Table S1: SUV- and MTR-based values with breast cancer subtypes; Figure S1: Box plots of selected MTR- and SUV-based parameters stratified by receptor status.

Author Contributions: Conceptualization, Y.K. and J.W.; methodology, Y.K. and J.W.; investigation, Y.K., Y.-F.T., L.-M.T., K.-H.L. and J.W.; formal analysis, L.-Y.L., Y.K., T.T.-F.S. and J.W.; writing—original draft preparation, L.-Y.L. and J.W.; writing—review and editing, L.-Y.L. and J.W.; supervision, J.W. All authors have read and agreed to the published version of the manuscript.

Funding: This research was funded by the Ministry of Health and Welfare (grant number MOHW109-TDU-B-212-010001), Taipei Veterans General Hospital (grant number V110C-031), the National Science and Technology Council (grant number NSTC 110-2314-B-075-033-), and the Melissa Lee Cancer Foundation (grant numbers MLCF-V111_A11104 and MLCF_V110_11004).

Institutional Review Board Statement: The study was conducted in accordance with the Declaration of Helsinki and approved by the Institutional Review Board of Taipei Veterans General Hospital (protocol code 2017-03-002A; date of approval: 21 March 2017). Patient recruitment for the present substudy began in January 2019, after the CEST imaging license became available; no protocol amendments were made during this interval.

Informed Consent Statement: Written informed consent was obtained from all patients involved in the study.

Data Availability Statement: The data presented in this study are available on request from the corresponding author due to patient privacy and confidentiality restrictions.

Acknowledgments: The authors thank Chien-Yuan Lin and Chia-Wei Lee, imaging scientists at GE Healthcare, for technical assistance in quantitative data extraction and organization.

Conflicts of Interest: The authors declare no conflicts of interest.

Abbreviations

NAC	Neoadjuvant chemotherapy
FDG	F-18 fluorodeoxyglucose
PET	Positron emission tomography
SUV	Standardized uptake value
TLG	Total lesion glycolysis
DCE	Dynamic contrast-enhanced
DWI	Diffusion-weighted imaging
ADC	Apparent diffusion coefficient
MRS	Magnetic resonance spectroscopy
ROC	Receiver operating characteristic
AUC	Area under the ROC curve
LOOCV	Leave-one-out cross-validation
MTI	Magnetization transfer imaging
MTR	Magnetization transfer ratio
pCR	Pathologic complete response
TNBC	Triple-negative breast cancer
HER2	Human epidermal growth factor receptor 2
ER	Estrogen receptor
PR	Progesterone receptor
HR	Hormone receptor
RCB	Residual cancer burden
PPV	Positive predictive value
NPV	Negative predictive value

References

1. Cho, N.; Im, S.A.; Kang, K.W.; Park, I.A.; Song, I.C.; Lee, K.H.; Kim, T.Y.; Lee, H.; Chun, I.K.; Yoon, H.J.; et al. Early prediction of response to neoadjuvant chemotherapy in breast cancer patients: Comparison of single-voxel (1)H-magnetic resonance spectroscopy and (18)F-fluorodeoxyglucose positron emission tomography. *Eur. Radiol.* **2016**, *26*, 2279–2290. [CrossRef]
2. Cho, N.; Im, S.-A.; Cheon, G.J.; Park, I.-A.; Lee, K.-H.; Kim, T.-Y.; Kim, Y.S.; Kwon, B.R.; Lee, J.M.; Suh, H.Y.; et al. Integrated 18F-FDG PET/MRI in breast cancer: Early prediction of response to neoadjuvant chemotherapy. *Eur. J. Nucl. Med. Mol. Imaging* **2018**, *45*, 328–339. [CrossRef]
3. Choi, E.K.; Yoo, I.R.; Kim, S.H.; Park, S.Y.; O, J.H.; Kang, B.J. The value of pre- and post-neoadjuvant chemotherapy F-18 FDG PET/CT scans in breast cancer: Comparison with MRI. *Acta Radiol.* **2018**, *59*, 41–49. [CrossRef]
4. de Mooij, C.M.; van Nijnatten, T.J.A.; Goorts, B.; Kooreman, L.F.S.; Raymakers, I.W.M.; van Meijl, S.P.L.; de Boer, M.; Keymeulen, K.; Wildberger, J.E.; Mottaghy, F.M.; et al. Prediction of Primary Tumour and Axillary Lymph Node Response to Neoadjuvant Chemo(Targeted) Therapy with Dedicated Breast [18F]FDG PET/MRI in Breast Cancer. *Cancers* **2023**, *15*, 401. [CrossRef]
5. Ghanikolahloo, M.; Taher, H.J.; Abdullah, A.D.; Asadi Anar, M.; Tayebi, A.; Rahimi, R.; Olamaeian, F.; Rahimikashkooli, N.; Kargar, N. The role of (18)F-FDG PET/MRI in assessing pathological complete response to neoadjuvant chemotherapy in patients with breast cancer: A systematic review and meta-analysis. *Radiat. Oncol.* **2024**, *19*, 164. [CrossRef]
6. Pahk, K.; Kim, S.; Choe, J.G. Early prediction of pathological complete response in luminal B type neoadjuvant chemotherapy-treated breast cancer patients: Comparison between interim 18F-FDG PET/CT and MRI. *Nucl. Med. Commun.* **2015**, *36*, 887–891. [CrossRef]
7. Tateishi, U.; Miyake, M.; Nagaoka, T.; Terauchi, T.; Kubota, K.; Kinoshita, T.; Daisaki, H.; Macapinlac, H.A. Neoadjuvant chemotherapy in breast cancer: Prediction of pathologic response with PET/CT and dynamic contrast-enhanced MR imaging—Prospective assessment. *Radiology* **2012**, *263*, 53–63. [CrossRef]
8. Umutlu, L.; Kirchner, J.; Bruckmann, N.M.; Morawitz, J.; Antoch, G.; Ting, S.; Bittner, A.K.; Hoffmann, O.; Häberle, L.; Ruckhäberle, E.; et al. Multiparametric (18)F-FDG PET/MRI-Based Radiomics for Prediction of Pathological Complete Response to Neoadjuvant Chemotherapy in Breast Cancer. *Cancers* **2022**, *14*, 1727. [CrossRef]
9. Wang, J.; Shih, T.T.; Yen, R.F. Multiparametric Evaluation of Treatment Response to Neoadjuvant Chemotherapy in Breast Cancer Using Integrated PET/MR. *Clin. Nucl. Med.* **2017**, *42*, 506–513. [CrossRef]
10. Caracciolo, M.; Castello, A.; Urso, L.; Borgia, F.; Marzola, M.C.; Uccelli, L.; Cittanti, C.; Bartolomei, M.; Castellani, M.; Lopci, E. Comparison of MRI vs. [(18)F]FDG PET/CT for Treatment Response Evaluation of Primary Breast Cancer after Neoadjuvant Chemotherapy: Literature Review and Future Perspectives. *J. Clin. Med.* **2023**, *12*, 5355. [CrossRef]

11. Baysal, H.; Serdaroglu, A.Y.; Ozemir, I.A.; Baysal, B.; Gungor, S.; Erol, C.I.; Ozsoy, M.S.; Ekinci, O.; Alimoglu, O. Comparison of Magnetic Resonance Imaging With Positron Emission Tomography/Computed Tomography in the Evaluation of Response to Neoadjuvant Therapy of Breast Cancer. *J. Surg. Res.* **2022**, *278*, 223–232. [CrossRef]
12. Pengel, K.E.; Koolen, B.B.; Loo, C.E.; Vogel, W.V.; Wesseling, J.; Lips, E.H.; Rutgers, E.J.T.; Valdés Olmos, R.A.; Vrancken Peeters, M.J.T.F.D.; Rodenhuis, S.; et al. Combined use of 18F-FDG PET/CT and MRI for response monitoring of breast cancer during neoadjuvant chemotherapy. *Eur. J. Nucl. Med. Mol. Imaging* **2014**, *41*, 1515–1524. [CrossRef]
13. Schmitz, A.M.T.; Teixeira, S.C.; Pengel, K.E.; Loo, C.E.; Vogel, W.V.; Wesseling, J.; Rutgers, E.J.T.; Valdés Olmos, R.A.; Sonke, G.S.; Rodenhuis, S.; et al. Monitoring tumor response to neoadjuvant chemotherapy using MRI and 18F-FDG PET/CT in breast cancer subtypes. *PLoS ONE* **2017**, *12*, e0176782. [CrossRef]
14. Tokuda, Y.; Yanagawa, M.; Fujita, Y.; Honma, K.; Tanei, T.; Shimoda, M.; Miyake, T.; Naoi, Y.; Kim, S.J.; Shimazu, K.; et al. Prediction of pathological complete response after neoadjuvant chemotherapy in breast cancer: Comparison of diagnostic performances of dedicated breast PET, whole-body PET, and dynamic contrast-enhanced MRI. *Breast Cancer Res. Treat.* **2021**, *188*, 107–115. [CrossRef]
15. McDonald, E.S.; Kazerouni, A.S.; Metanet, P.; Barinov, L.; Partridge, S.C.; Hylton, N.M. The Future of Quantitative Breast Imaging: Integrated to Integral Imaging Biomarkers for Precision Cancer Care, From the AJR Special Series on Quantitative Imaging. *Am. J. Roentgenol.* **2026**. [CrossRef]
16. Arlinghaus, L.R.; Dortch, R.D.; Whisenant, J.G.; Kang, H.; Abramson, R.G.; Yankeelov, T.E. Quantitative Magnetization Transfer Imaging of the Breast at 3.0 T: Reproducibility in Healthy Volunteers. *Tomography* **2016**, *2*, 260–266. [CrossRef]
17. Bonini, R.H.; Zeotti, D.; Saraiva, L.A.; Trad, C.S.; Filho, J.M.; Carrara, H.H.; de Andrade, J.M.; Santos, A.C.; Muglia, V.F. Magnetization transfer ratio as a predictor of malignancy in breast lesions: Preliminary results. *Magn. Reson. Med.* **2008**, *59*, 1030–1034. [CrossRef]
18. Heller, S.L.; Moy, L.; Lavianlivi, S.; Moccaldi, M.; Kim, S. Differentiation of malignant and benign breast lesions using magnetization transfer imaging and dynamic contrast-enhanced MRI. *J. Magn. Reson. Imaging* **2013**, *37*, 138–145. [CrossRef]
19. Henkelman, R.M.; Stanisz, G.J.; Graham, S.J. Magnetization transfer in MRI: A review. *NMR Biomed.* **2001**, *14*, 57–64. [CrossRef]
20. Oreja-Guevara, C.; Charil, A.; Caputo, D.; Cavarretta, R.; Sormani, M.P.; Filippi, M. Magnetization transfer magnetic resonance imaging and clinical changes in patients with relapsing-remitting multiple sclerosis. *Arch. Neurol.* **2006**, *63*, 736–740. [CrossRef]
21. York, E.N.; Thrippleton, M.J.; Meijboom, R.; Hunt, D.P.J.; Waldman, A.D. Quantitative magnetization transfer imaging in relapsing-remitting multiple sclerosis: A systematic review and meta-analysis. *Brain Commun.* **2022**, *4*, fcac088. [CrossRef]
22. Virostko, J.; Sorace, A.G.; Wu, C.; Ekrut, D.; Jarrett, A.M.; Upadhyaya, R.M.; Avery, S.; Patt, D.; Goodgame, B.; Yankeelov, T.E. Magnetization Transfer MRI of Breast Cancer in the Community Setting: Reproducibility and Preliminary Results in Neoadjuvant Therapy. *Tomography* **2019**, *5*, 44–52. [CrossRef]
23. Lombardi, A.; Lazzeroni, R.; Bersigotti, L.; Vitale, V.; Amanti, C. The Proper Ki-67 Cut-Off in Hormone Responsive Breast Cancer: A Monoinstitutional Analysis with Long-Term Follow-Up. *Breast Cancer* **2021**, *13*, 213–217. [CrossRef]
24. Fujii, T.; Kogawa, T.; Dong, W.; Sahin, A.A.; Moulder, S.; Litton, J.K.; Tripathy, D.; Iwamoto, T.; Hunt, K.K.; Pusztai, L.; et al. Revisiting the definition of estrogen receptor positivity in HER2-negative primary breast cancer. *Ann. Oncol.* **2017**, *28*, 2420–2428. [CrossRef]
25. de Mooij, C.M.; Ploumen, R.A.W.; Nelemans, P.J.; Mottaghy, F.M.; Smidt, M.L.; van Nijnatten, T.J.A. The influence of receptor expression and clinical subtypes on baseline [18F]FDG uptake in breast cancer: Systematic review and meta-analysis. *EJNMMI Res.* **2023**, *13*, 5. [CrossRef]
26. Abubakar, Z.A.; Akepati, N.K.R.; Bikkina, P. Correlation of Maximum Standardized Uptake Values in 18F-Fluorodeoxyglucose Positron Emission Tomography-computed Tomography Scan with Immunohistochemistry and Other Prognostic Factors in Breast Cancer. *Indian J. Nucl. Med.* **2019**, *34*, 10–13. [CrossRef]
27. Baba, S.; Isoda, T.; Maruoka, Y.; Kitamura, Y.; Sasaki, M.; Yoshida, T.; Honda, H. Diagnostic and prognostic value of pretreatment SUV in 18F-FDG/PET in breast cancer: Comparison with apparent diffusion coefficient from diffusion-weighted MR imaging. *J. Nucl. Med.* **2014**, *55*, 736–742. [CrossRef]
28. Boellaard, R.; Herrmann, K.; Barrington, S.F.; Cranston, I.; Mottaghy, F.M.; Hoekstra, C.J.; Beyer, T.; Pike, L.C.; Willemsen, A.T.M.; Graham, M.M.; et al. [18F]FDG PET/CT: EANM procedure guidelines for tumour imaging: Version 3.0. *EANM J.* **2025**, *1*, 100006. [CrossRef]
29. Krokos, G.; MacKewn, J.; Dunn, J.; Marsden, P. A review of PET attenuation correction methods for PET-MR. *EJNMMI Phys.* **2023**, *10*, 52. [CrossRef]

Disclaimer/Publisher's Note: The statements, opinions and data contained in all publications are solely those of the individual author(s) and contributor(s) and not of MDPI and/or the editor(s). MDPI and/or the editor(s) disclaim responsibility for any injury to people or property resulting from any ideas, methods, instructions or products referred to in the content.